HEFAT2011
8th International Conference on Heat Transfer, Fluid Mechanics and Thermodynamics
11 – 13 July 2011
Pointe Aux Piments, Mauritius

LIVE EXPERIMENTS ON MELT BEHAVIOR IN THE REACTOR PRESSURE VESSEL LOWER HEAD

Miassoedov A.*, Cron T., Gaus-Liu X., Palagin A., Schmidt-Stiefel S., Wenz T.
*Author for correspondence
Karlsruhe Institute of Technology
Hermann-von-Helmholtz-Platz 1, D-76344 Eggenstein-Leopoldshafen,
Germany,
E-mail: alexei.miassoedov@kit.edu

ABSTRACT

Behavior of the corium pool in the lower head is still a critical issue in understanding of Pressurized Water Reactor (PWR) core meltdown accidents. One of the key parameter for assessing the vessel mechanical strength is the resulting heat flux at the pool-vessel interface. A number of studies [1]-[3] have already been performed to pursue the understanding of a severe accident with core melting, its course, major critical phases and timing and the influence of these processes on the accident progression. Uncertainties in modeling these phenomena and in the application to reactor scale will undoubtedly persist. These include e.g. formation and growth of the in-core melt pool, relocation of molten material after the failure of the surrounding crust, characteristics of corium arrival in residual water in the lower head, corium stratifications in the lower head after the debris re-melting [4]. These phenomena have a strong impact on a potential termination of a severe accident.

The main objective of the LIVE program [5] at Karlsruhe Institute of Technology (KIT) is to study the core melt phenomena both experimentally in large-scale 3D geometry and in supporting separate-effects tests, and analytically using CFD codes in order to provide a reasonable estimate of the remaining uncertainty band under the aspect of safety assessment. Within the LIVE experimental program several tests have been performed with water and with non-eutectic melts (mixture of KNO_3 and $NaNO_3$) as simulant fluids. The results of these experiments, performed in nearly adiabatic and in isothermal conditions, allow a direct comparison with findings obtained earlier in other experimental programs (SIMECO, ACOPO, BALI, etc.) and will be used for the assessment of the correlations derived for the molten pool behavior.

The information obtained from the LIVE experiments includes heat flux distribution through the reactor pressure vessel wall in transient and steady state conditions, crust growth velocity and dependence of the crust formation on the heat flux distribution through the vessel wall. Supporting post-test analysis contributes to characterization of solidification processes of binary non-eutectic melts. Complimentary to other international programs with real corium melts, the results of the LIVE activities provide data for a better understanding of in-core corium pool behavior. The experimental results are being used for development of mechanistic models to describe the in-core molten pool behavior and their implementation in the severe accident codes like ASTEC.

The paper summarizes the objectives of the LIVE program and presents the main results obtained in the LIVE experiments up to now.

INTRODUCTION

The sequence of a postulated core melt down accident in the reactor pressure vessel (RPV) of Light Water Reactors (LWR) involves a large number of complex physical and chemical phenomena, and strongly depends on the accident sequence and the considered reactor design.

In-vessel core melt progression can be divided into the "early" and the "late" phase. While detailed experimental and theoretical information about the early phase is available, large uncertainties exist in the modeling of the late phase, which is characterized by substantial melting of fuel, formation of melt pools, and melt accumulation in the lower head of the RPV. Steady state behavior of debris and of molten pools in the lower head has been investigated in several experimental studies. However, the database for the transient processes during core melting, melt relocation and accumulation is still very limited. For the melt released into the lower head of the vessel, there is a lack of information about e.g. transient heat fluxes through the vessel wall, crust formation, stability and re-melting in 3D geometry.

For instance, regarding experiments in large scale geometry using water as simulant, COPO II [6] and BALI [7]

experiments performed in 2D slice geometry showed clearly higher heat transfer coefficients (20-30%) for the side and bottom boundaries than those in the 3D ACOPO experiments [3], while the upward heat transfer coefficients were only slightly higher. This implies a different top to downward split, which in the reactor case would be important e.g. for the amount of heat transferred to an overlying metallic layer and thus the strength of the focusing effect. Several reason for the differences have been discussed, mainly related to the presence of a frozen boundary in COPO II and BALI as compared to ACOPO, including importance of an isothermal boundary, surface roughness of the crust or non-linearity in fluid properties due to larger temperature differences between pool and boundary. Clear conclusion could not yet be drawn.

Another yet unresolved question is related to the existence of mushy layers or sharp interfacial boundaries along crust boundaries in the case of non-eutectic melt. Different approaches exist, either assuming a mushy layer with larger temperature differences between melt bulk and pool boundary, but smaller heat transfer coefficients due to increased viscosity caused by solid fractions, or sharp liquid/solid boundaries with the surface temperature at liquidus temperature, thus smaller temperature differences but larger heat transfer coefficients. The experimental and theoretical studies performed up to now did not yield a decision yet.

An improved understanding of these processes can help to define accident management procedures for accident control in present reactors. In order to address these questions and to complement the experimental data on melt pool behavior in the vessel lower head, KIT performs large-scale tests through the LIVE (Late In-Vessel Phase Experiments) program. The LIVE tests are designed to investigate the core melt behavior in the lower plenum of the reactor pressure vessel and the influence of the cooling of the vessel outer surface with water in the conditions that may occur during core meltdown accident in PWRs. To simulate the corium melt a non-eutectic binary mixture of $NaNO_3$ and KNO_3 is used.

The information obtained from the LIVE experiments includes the melt temperature evolution during different stages of the test, the heat flux distribution along the reactor pressure vessel wall in transient and steady state conditions, the crust growth velocity and the influence of the crust formation on the heat flux distribution along the vessel wall. In the post-test analysis crust thickness profile along the vessel wall, the crust composition and the morphology are determined.

The experimental results are being used for the development of mechanistic models for the description of in-core molten pool behavior and their implementation in severe accident codes. Different models are applied for post-test calculations and comparative analyses. These include simplified, but fast running models implemented in the severe accident codes ASTEC [8], ATHLET-CD and a computational tool developed at the Royal Institute of Technology Stockholm (PECM model implemented in Fluent) [9]. The calculations are complemented by analyses with the CFD code CONV (thermal hydraulics of heterogeneous, viscous and heat-generating melts) [10] which was developed at IBRAE (Nuclear Safety Institute of Russian Academy) within the RASPLAV project and was further improved within the ISTC 2936 Project.

The paper summarizes the objectives of the LIVE program and presents the main results obtained in the LIVE experiments up to now.

EXPERIMENTAL SET-UP

The main part of the LIVE test facility is a 1:5 scaled Reactor Pressure Vessel of a typical pressurized water reactor (Figure 1). The inner diameter of the test vessel is 1 m and the wall thickness is 25 mm. The material of the test vessel is stainless steel.

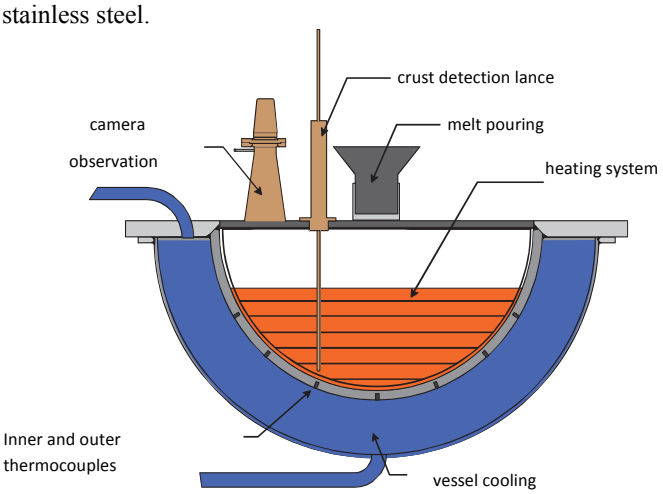

Figure 1 Test vessel of the LIVE facility

Decay power input into the melt is recorded and melt samples are extracted during the tests. Different openings in the upper lid of the test vessel allow pouring of the melt to the central region or close to the perimeter of the lower head. To be able to investigate the crust, which is formed at the wall of the vessel, the residual melt is extracted from the vessel at the end of the test to uncover the crust.

To investigate the influence of different external cooling conditions on the melt pool behavior, the test vessel is enclosed by a second vessel (cooling vessel) to be able to cool the test vessel at the outside. The cooling water inlet is located at the bottom of the cooling vessel and the outlet is positioned at the top of the vessel.

The volumetric heating system has to simulate the decay heat released from the corium melt. Consequently, the heating system has to produce the heat in the melt as homogeneously as possible. Therefore a heater grid with several independent heating elements was constructed (Figure 2). The heating elements are shrouded electrical resistance wires. The maximum temperature the heating system can provide is limited to 1100 °C. To allow the homogeneous heating of the melt pool, the heating system has six heating planes at different elevations with a distance of about 45 mm. Each heating plane consists of a spirally formed heating element with a distance of ~40 mm between each winding. The heating elements are

located in a special cage to ensure the correct positioning. All heating planes together provide a maximum power of about 28 kW. Each plane can be controlled separately to allow the homogeneous heat release in the melt.

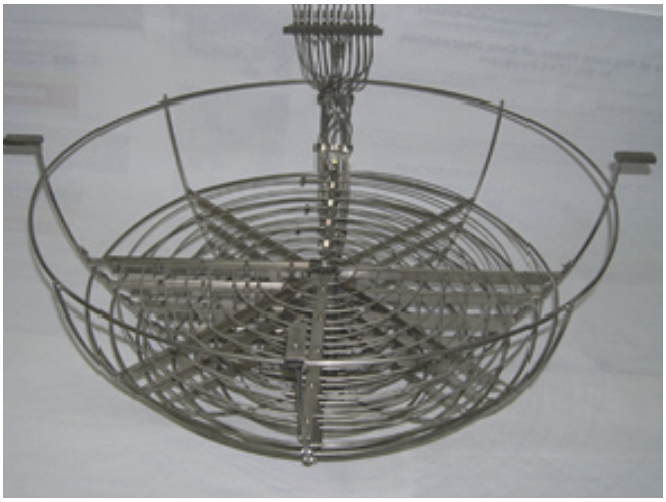

Figure 2 LIVE volumetric heating system

Simulant materials used in the LIVE program should, to the greatest extent possible, represent the real core materials in important physical properties and in thermo-dynamic and thermo-hydraulic behavior. Therefore, the applicability of several binary melt compositions as a simulant for the oxidic part of the corium has been investigated.

Important criteria for the selection are that the simulant melt should be a non-eutectic mixture of several components with a distinctive solidus-liquidus area of about 100 K, and that the simulant melt should have a similar solidification and crust formation behavior as the oxidic corium.

In the LIVE-L6 experiment a binary mixture of sodium nitrate $NaNO_3$ and potassium nitrate KNO_3 was chosen. The eutectic composition of this melt is 50-50 mole% and the eutectic temperature is 225 °C (Figure 3). The maximum temperature range between solidus and liquidus is ~60 K and corresponds to a 20-80 mole% $NaNO_3$-KNO_3 mixture (Levin, 1986). This melt can be used in a temperature range from 220 °C (solidification) to 380 °C (chemical decomposition). Due to its solubility for water the applicability of this melt is restricted to dry conditions inside the test vessel.

To investigate both the transient and the steady state behavior of the simulated corium melt, an extensive instrumentation of the test vessel is realized. Seventeen thermocouples are installed at five levels and along four azimuth angles on the inner wall surface of the test vessel and 17 thermocouples at the same positions on the outer wall surface. Based on the temperature measurements it is possible to calculate heat fluxes at these positions. Furthermore, 36 thermocouples are located inside the melt pool to measure the melt pool temperatures at different positions. The copper plate used to separate the two layers of the melt is 2 mm thick and is located at the vessel height of 333 mm. Two thermocouples are installed at the top and the bottom of the plate, and a thermocouple tree with 10 thermocouples, each in 10 mm distance, is mounted at the bottom of the plate to measure the melt temperature below the plate. Three thermocouple trees are installed on the vessel wall to quantify the crust growth. Each thermocouple tree consists of 7 thermocouples, which are arranged parallel to the vessel wall. The distance between the thermocouples varies between 9 and 3 mm. At the outer surface of the cooling tank three thermocouples are installed to measure the temperature between the cooling tank and the insulation layer.

The melt pool vertical temperature profile and the boundary temperature at the melt/crust interface are measured by the crust detection system. The measuring lance is attached to the linear actuator. The lance can be driven downwards to the melt at 0.1mm accuracy.

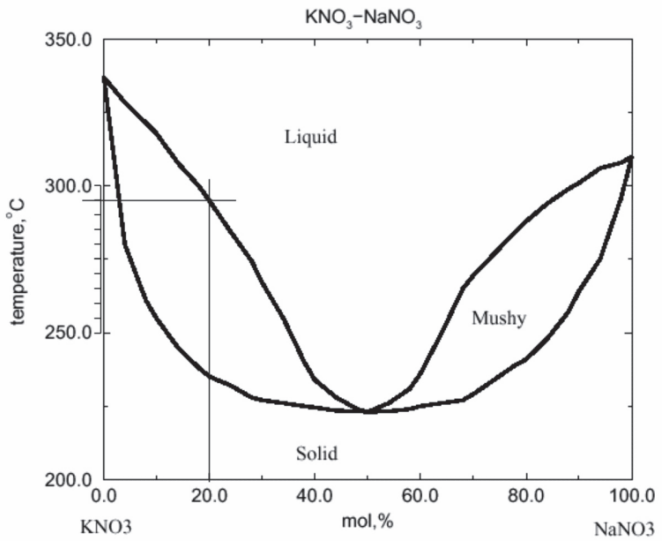

Figure 3 KNO_3-$NaNo_3$ phase diagram

EXPERIMENTAL SET-UP

Ten experiments were performed in the LIVE facility up to now with different initial and boundary conditions. The main parameters of the tests are the following:

- mass of melt: either 120 l of melt in tests L1, L2, L3 and L3A or 210 l in tests L4, L5L, L9 and L9A were used. Scaled to the reactor case, the mass of melt corresponds to 70% and 100% of the total core inventory respectively.
- cooling condition: for the tests with 120 l melt, initial external air cooling and then water flooding after 2 hours was performed in L1 and L3 test; whereas external water cooling was performed from the beginning to the end in all other tests.
- melt pour position: the melt was poured near the vessel wall at 157.5° azimuth angle in the tests L3, L3A and the second pour of L5L, in other tests the melt was poured centrally.

- simulant melt composition: eutectic melt of 50 mole% KNO_3 - 50 mole% $NaNO_3$ with a melting temperature of 224°C was applied in L9 and L9A, whereas a non-eutectic melt of 80 mole% KNO_3 - 20 mole% $NaNO_3$ with melting temperature range of 284°C-224°C was applied in other tests.
- initial melt temperature: in the tests with non-eutectic melts the initial melt temperature was 66°C above melting temperature, whereas in the tests with eutectic melts, the initial melt temperature was either 125°C above melting temperature (L9) or 75°C above melting temperature (L9A).
- heating power: in most tests more than one heating plateau was applied. Each heating period lasted several hours so that the thermal-hydraulic steady state in the vessel was assumed to be achieved. For the mass amount of 120 l, 10 kW and then 7 kW were applied, whereas for the mass amount of 210 l, five heating plateaux of the order of 18 kW, 10 kW, 5 kW, 10 kW, 18 kW (15 kW in L4) were applied.

Main results of the experiments are summarized below.

Influence of heat generation

The influence of different heat generations on melt temperature, heat flux distribution in thermal hydraulic steady state of LIVE cases is investigated. Other test conditions are identical and are referred to as standard test conditions in this study which means the special influence of the cooling condition and melt pour position is not considered. The standard test conditions are:

- external water cooling at the begin of the test before the melt pour;
- central melt pour;
- non-eutectic melt;
- initial melt temperature /maximum temperature above liquidus temperature T_{liq}: 350°C/66°C.

The influence of heat generation rate was investigated in the L4 test. Four heat generation levels in the sequence of 18 kW, 15 kW, 10 kW and 5kW for heating of 210 l melt were applied. The height of melt pool was 425 mm, and Ra number during 18 kW heating period was assumed to be 4.46×10^{13} and Ra number during 5 kW heating period was assumed to be 1.21×10^{13}.

Figure 4 shows the melt temperature at different vessel heights during different heat generations. The temperature points in Figure 4 (a) were measured by thermal couples located at radius 74 mm in L4 test; the temperature profiles shown in Figure 4 (b) were obtained by a crust detecting lance during the L5 test which intruded into the melt at the radius 365 mm from the axis. The results demonstrate that increasing heating power led to increase of overall melt temperature in the melt pool. Increasing the heating power also resulted in the shifting the maximum melt temperature upwards to the melt surface. Figure 4 (b) reveals the detailed melt temperature distributions during different heating powers. A temperature boundary layer of ~4 mm was detected adjacent to the crust/melt interface. The temperature gradient within the boundary layer during 18 kW heating power was about 9 °C/mm. Adjoining this boundary layer a region with violently fluctuating temperature was observed which is caused by a downward flow of colder melt. Above this region there was a stagnant zone with increasing temperature upwards and a turbulent zone with nearly homogeneous melt temperature.

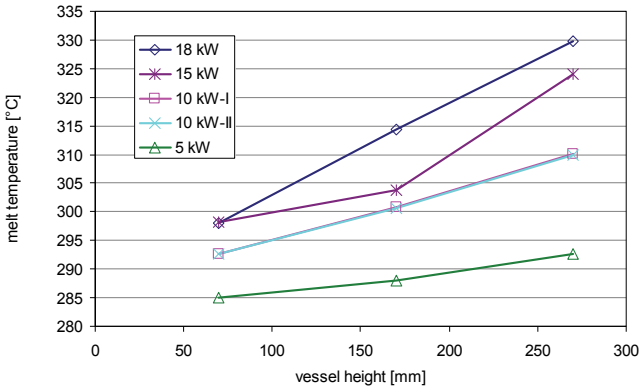

a)

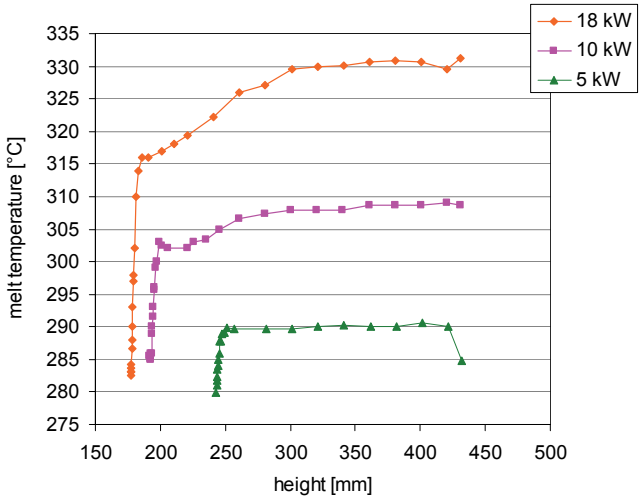

b)

Figure 4 (a) Melt temperature dependence on vessel height in the L4 test, 74 mm from axis; (b) melt temperature vertical profile in the L5L test, 365 mm from axis

The vertical distribution of heat flux through the vessel sidewall is shown in Figure 5. Increasing heating power intensified the focusing of heat flux towards the melt surface. At the lower part of the melt pool, which is located below 30° polar angle, the heat fluxes were low and remained almost unchanged during different heat generation levels.

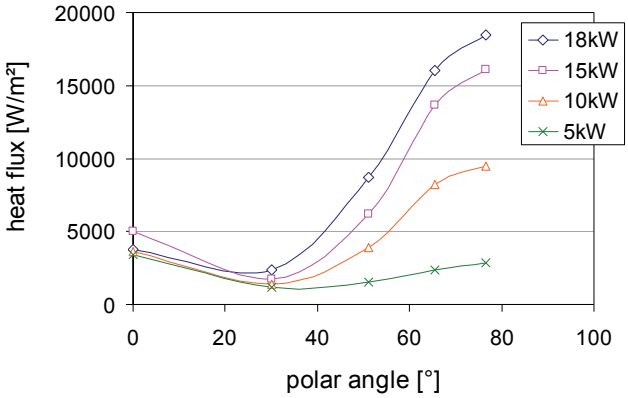

Figure 5 Heat flux distribution along vessel height under different heat generation levels

Influence of initial cooling condition

Two cooling conditions are considered in this study: one is the water cooling, which means water is injected into in the cooling vessel and a certain flow rate of cooling water is applied already at the beginning of melt pour. The other one is the delayed water cooling, which means the vessel is air cooled during the first two hours after melt pour, and then the test vessel was externally water cooled till the end of the test. In case of the delayed water cooling (L1 and L3 tests), the air cooling could not cool the melt pool sufficiently to reach steady state conditions. As a result, the melt temperatures increased continuously and the upper part of the crust formed at the vessel inner wall surface was completely molten. After water flooding a new crust layer was built up under low cooling rate. In contrast, water cooling from the beginning of melt pour could reduce the melt pool temperature efficiently.

Different cooling condition resulted in different crust growth rates and crust thermal conductivity. The crust growth rates under different initial cooling conditions during the 10 kW heating power period are compared. Figure 6 shows the crust growth rate at the polar angle 52.9° under the delayed water cooling (L3) and under the initial water cooling (L3A) conditions. The melt solidified significantly faster under the initial water cooling condition than under delayed water flooding during the initial period and the crust growth period was shorter under water cooling condition.

Thermal conductivity of the crust corresponded adversely to the crust growth rate. As it is shown in Figure 7, the crust layer formed during the initial water cooling (L3A test) has lower thermal conductivity than the one formed during delayed water cooling condition (L3 test). The difference in thermal conductivity can be traced back to the crust morphology and crust porosity which are strongly dependent on the solidification rate.

Dependent on the crust thermal conductivity the final crust layer thickness in steady state should be different for the same local heat fluxes. This was confirmed by the measurements indicating that the final crust layer formed under water cooling condition was thinner than the one formed under delayed water cooling condition. These results demonstrate the influence of the solidification parameters: initial cooling conditions determine the solidification rate, which leads to different microstructure and porosity of the crust. The microstructure of the crust exerts strong influence on the crust thermal conductivity and the final crust thickness. This phenomenon observed for the simulant melt implies a general character of the solidification process of non-eutectic melts, which could also appear in corium melt. Certainly the influence of the cooling condition on solid crust properties for the corium melt can only be quantified with experiments using prototypical materials.

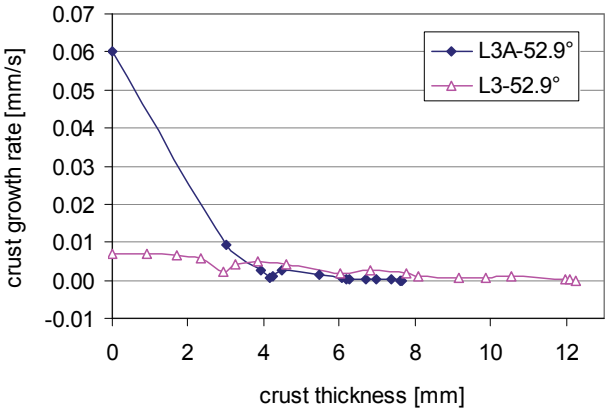

Figure 6 Crust growth rate under different initial cooling condition at the polar angle 52.9°

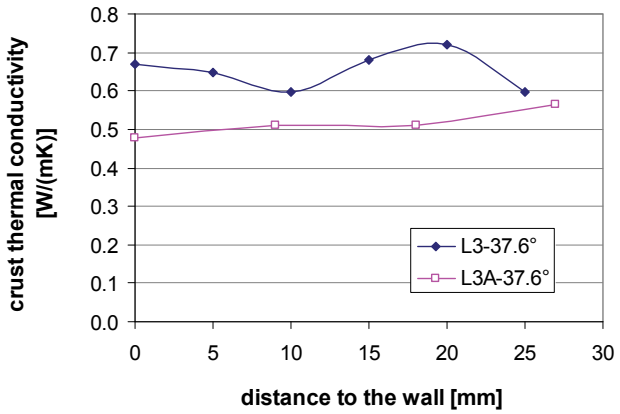

Figure 7 Crust thermal conductivity at the polar angle of 37.6°

Influence of melt composition

Two tests with identical initial and boundary conditions were performed with eutectic (L9) and non-eutectic (L4) melts. Besides the difference in melting temperature, the differences in the solidification process and in the crust microstructure are well known:

- during the solidification of non-eutectic melt, the crust/melt interface temperature is lower than the bulk melt liquidus

temperature; if the melt is undercooled, a mushy zone exists and the front of the solid shows cellular or dendrite structure;

- during the solidification of the eutectic melt, the crust/melt interface temperature remains constant at the melting temperature, a planar front exists, the solid presents fine grains and there is no macro-segregation of melt components [13].

Corresponding to the liquidus temperature of the eutectic melt, the melt temperature in the test of eutectic material (L9) was generally ~ 60 °C lower than the one of non-eutectic test. However, the heat flux distributions through the vessel sidewall of the two tests are comparable. In Figure 8 the heat fluxes through the vessel height during 18 kW heating period are shown. It is also notable that the final crust thickness profiles of the two tests were similar, but the crust thermal conductivities were quite different.

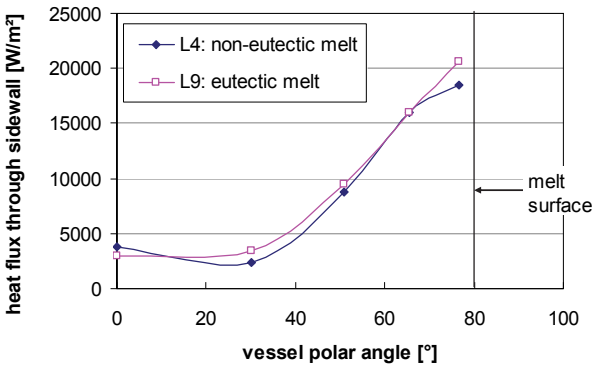

Figure 8 Heat flux through vessel sidewall from L9 and L4

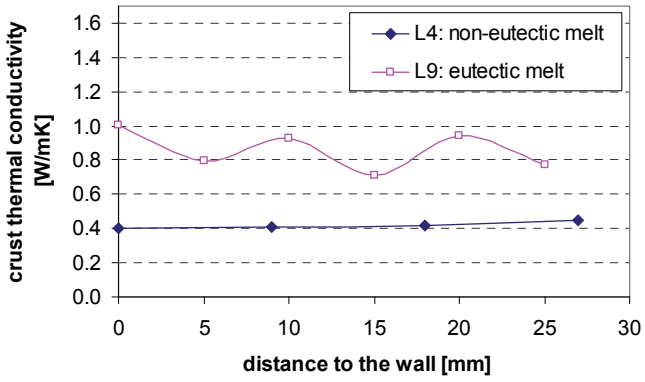

Figure 9 Crust thermal conductivity from L4 and L9 test at polar angle of 37.6°

As it is shown in Figure 9, the thermal conductivity of the eutectic crust was considerable higher than the one of the non-eutectic crust. The post-test porosity analysis reveals that the mean value for the porosity of eutectic crust is 2.6%, whereas the mean value for the porosity of non-eutectic crust is about 4.8%. The compact microstructure of the eutectic crust is one of the reasons for the higher thermal conductivity of the eutectic solid material.

Influence of melt initial temperature

The impact of the initial melt temperature on the thermal hydraulic transient state and steady state was investigated in L9 and L9A tests using eutectic melt composition. The thermal hydraulic transient state means that the crust growth rate is greater than zero, whereas the thermal hydraulic steady state means that the crust growth rate is equal to zero. Therefore there is no mass transfer between the solid crust and liquid melt in steady state. The initial melt temperature in L9 and L9A was 350 °C and 300 °C respectively. Only 18 kW and 10 kW heating periods were performed in L9A test. Other test conditions of the two tests are identical.

During the steady state of the two tests, the melt temperature and the heat flux distribution through the vessel sidewall agreed very well with each other. The crust thickness during the same heating power was also comparable. However, some difference in melt behaviour during the transient state can be observed. In the case of higher initial melt temperature (L9), the transient heat flux through the side wall was higher and correspondingly more heat was removed through the vessel wall at the initial period of the test. Figure 10 shows the total heat removed through the vessel wall at the beginning of the test. The main portion of the excessive heat in L9 was transferred through the wall during the first hour after the melt pour.

Higher initial melt temperature led to a longer crust growth period. The crust growth periods in L9 were about twice as long as those in L9A test. It should be noted that in all LIVE tests, including those with non-eutectic composition, the crust growth period in the lower part of the melt pool was longer than in the upper part of the melt pool.

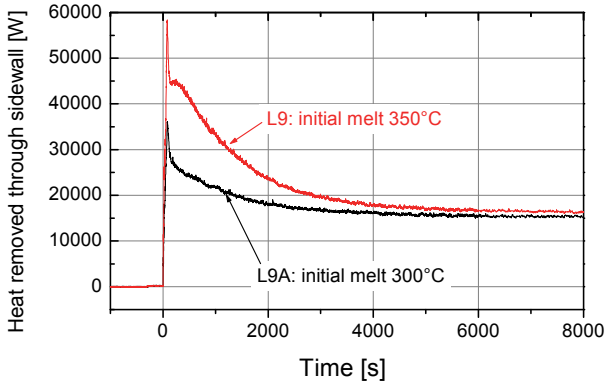

Figure 10 Heat removed through the vessel wall during the initial period of test

APPICATION OF THE CONV CODE TO LIVE TESTS

To simulate the LIVE experiments test the CONV code was used. CONV is a thermohydraulic CFD code for the simulation of heat transfer due to conduction and convection in complex geometry. It was developed at IBRAE (Nuclear Safety Institute of Russian Academy of Sciences, Moscow) within the framework of the International RASPLAV project to validate the concept of melt confinement in the reactor pressure vessel. For the modelling of heat generating viscous liquid in gravity field with consideration of the buoyancy force in a Bousinesque approximation the efficient difference scheme is applied to solve unsteady Navier-Stocks equations in natural "velocity-pressure" variables on fully staggered orthogonal grids for Cartesian coordinates. For the modeling of turbulence algebraic turbulent models were implemented in the code.

The CONV code was applied for the modeling of the LIVE-L4 test. An orthogonal curvi-linear grid with a nodalisation of 201×201 meshes was used in the calculations. The grid was refined near the liquid/solid boundary and near the upper surface of the liquid (Figure 11).

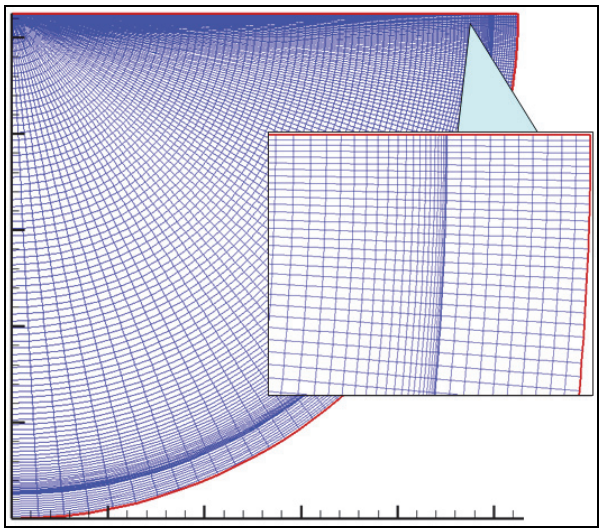

Figure 11 Type of nodalization scheme used in the calculations with CONV code

Two calculations were performed: a) assuming homogeneous heat generation in the melt pool and b) accounting for wire heaters used to simulate the heat generation in the melt. The following assumptions have been made:

- the heat flux from the upper surface was estimated from the experimental data and amount to ~70 Wt/m^2,
- the external cooling of the vessel outer wall surface was simulated using boundary conditions for the temperature and the heat transfer coefficients at different positions of the vessel wall derived from the test measurements,
- since the current code version can not model the solidification of binary mixtures, the temperature of 295 °C (liquidus) was used as a solidification temperature.

The following results obtained from the CONV calculation were compared with the experimental data:

- temperature distribution in the melt pool,
- heat flux distribution through the vessel wall,
- thickness of the crust at the vessel/melt pool interface at the end of the experiment.

The comparison of measured and calculated temperature evolution during the first three phases of the experiment (cooldown from 18 kW to 5 kW) in the upper half of the melt pool is given in Figure 12. Globally the experimental trend is obtained even if the calculated temperature deviates from the measured one by ~20 K. Generally, assuming the homogenous heat distribution in the melt leads to a slight underestimation of temperatures in the steady state phases of the test. In the contrary, when the heaters are modeled, the pool temperature is always overpredicted. This can be explained by the different heat generation density in the two considered cases. In the first case the heat is distributed homogeneously and in the second case only up to the level of 29 cm (location of the last heating plane).

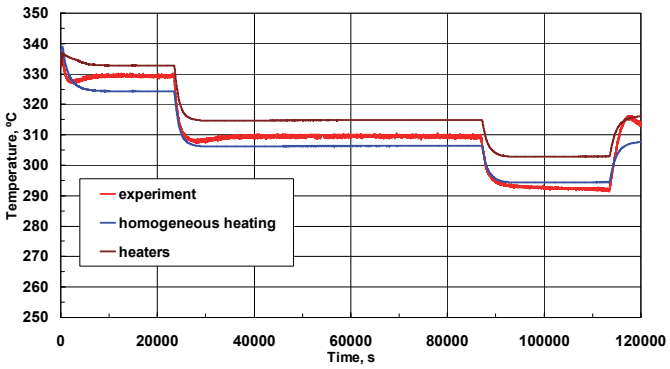

Figure 12 Measured and calculated temperature evolution in the melt during the first three phases of the LIVE-L4 test

The heat flux through the vessel wall is given in the Figure 13 for the first phase of the test with 18 kW heat generation. The results demonstrate that the difference between the two calculations is quite comparable with the experimental observations. However, at the angle range from 20° to 65° the second calculation overestimates the measured fluxes. At the angle above 65° the calculated heat flux is significantly lower than the measured one. This is consistent with the temperature distribution in the pool and can be explained by the different heat generation density, as in the case with the melt temperatures. Similar tendency was observed in all five phases of the experiment.

The crust thickness profile calculated for the first three phases of the test during the steady state is presented in the Figure 14. The code significantly underpredicts the experimentally determined values. Increasing the the crust thermal conductivity from 0.15 to 0.45 W/mK (blue line) did not improve the results. The obvious reason for this

underprediction is the limitation of the code which is not yet capable to simulate the solidification behaviour of binary non-eutectic melts. In these calculations the temperature of 295 °C (liquidus temperature of the melt composition) was used to track the crust front. Moreover, the code does not take into account the possible gap formation between the vessel wall and the solid crust which decreases the effective thermal conductivity of the crust/gap layer.

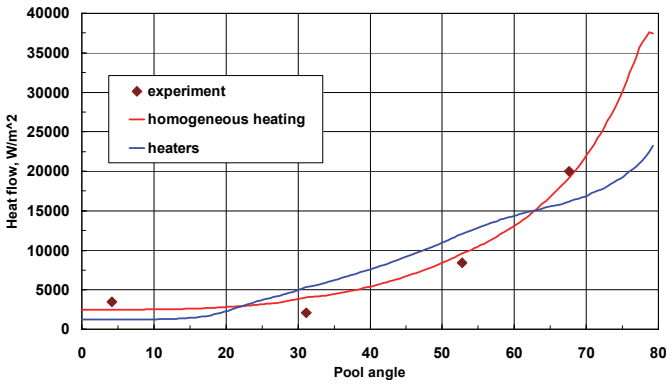

Figure 13 Heat flux distribution through the vessel wall during the first phase (18 kW) of the LIVE-L4 test

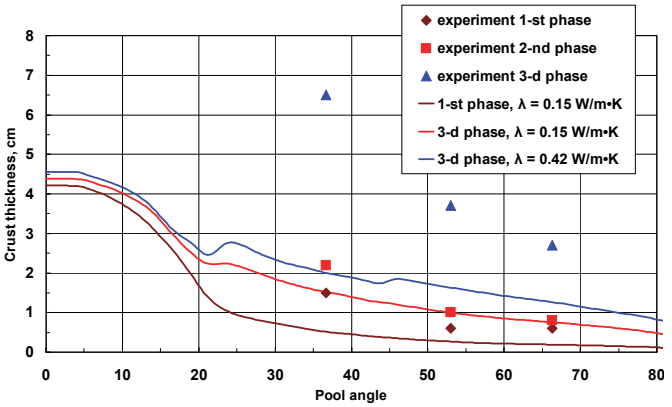

Figure 14 Comparison of the calculated and measured crust thickness profile in the LIVE-L4 test

The analysis of the LIVE-L4 with CONV code test showed that the experiment results can be quite accurately predicted by the CFD simulation. It is therefore expected to apply the CONV code to other high-temperature LIVE tests with molten salt and binary oxides including the modeling of solidification of binary non-eutectic melts providing valuable support for understanding and improvement of modeling in severe accident codes.

CONCLUSIONS

The large-scale tests performed at KIT through the LIVE program complement the experimental data on melt pool behavior. The tests are designed to support the analysis of core melt behavior in the lower plenum of the reactor pressure vessel and the influence of the cooling of the vessel outer surface with water in the conditions that may occur during core meltdown accident in PWRs.

Ten LIVE tests have been performed to investigate the melt pool transient and steady-state behaviour under different heating and cooling conditions. Comprehensive experimental results have been obtained regarding melt pool temperature, heat flux distribution through the vessel sidewall, crust thickness and crust properties. Furthermore, the influences of initial cooling conditions and initial melt temperature on the transient and steady state melt pool behaviour are studied. Both non-eutectic and eutectic melts were used and their solidification character and the behaviour of the melt pool are presented. In detail, the following conclusions can be drawn:

- increasing heating power in the melt intensifies the heat flux focusing at the melt surface;
- water cooling at the begin of the test before the melt pour leads to higher crust growth rates, lower crust thermal conductivities and thinner crust layers than delayed water cooling does;
- lower melting temperature of the eutectic melt leads to low melt pool temperature for the same heating power and melt mass. However, the heat flux distribution through the vessel wall in eutectic melt is comparable to that in non-eutectic melt. The final crust thicknesses are similar for both compositions, but the thermal conductivity of the eutectic crust is considerable higher than the one of the non-eutectic crust;
- higher initial melt temperatures lead to a longer crust growth period and longer times to reach the thermal hydraulic steady state conditions, but have only a small influence on the steady state melt pool behaviour.

The analysis of LIVE tests with CONV code test showed that the experiment results can be quite accurately predicted by the CFD simulation. It is therefore expected to apply the CONV code to other high-temperature LIVE tests with molten salt and binary oxides including the modeling of solidification of binary non-eutectic melts providing valuable support for understanding and improvement of modeling in severe accident codes.

REFERENCES

[1] Kymäläinen, O., et al., In-Vessel Retention of Corium at the Loviisa Plant, *Nuclear Engineering and Design*, 169, 1997, pp. 109-130.

[2] Alabin, S., et al., The Results and Analysis of the RASPLAV Salt Tests, *Proc. of the RASPLAV Seminar*, Munich, Germany, November 14-15, 2000.

[3] Theofanous, T. G, and Angelini, S., Natural Convection for In-Vessel Retention at Prototypic Rayleigh Numbers, *Nuclear Engineering and Design*, 200, 2001, pp. 1-9.

[4] Asmolov, V., et al., Challenges Left In the Area of In-Vessel Melt Retention, *Nuclear Engineering and Design*, 209, 2001, pp. 87-96.
[5] Fluhrer, B., et al., The Experimental Programme LIVE to Investigate In-Vessel Core Melt Behaviour in the Late Phase, *Proc. of the Jahrestagung Kerntechnik 2005*, INFORUM GmbH, Nürnberg, Germany, 2005, pp. 198-201.
[6] Helle, M., et al., Experimental Data on Heat Flux Distribution from a Volumetrically Heated Pool with Frozen Boundaries, *Proceedings of In-Vessel Core Debris Retention and Coolability Workshop*, Garching, Germany, March 3-6,1998, pp. 173-183.
[7] Bernaz, L., et al., Thermal Hydraulic Phenomena in Corium Pools: Numerical Simulation with TOLBIAC and Experimental Validation with BALI, *Proceedings of In-Vessel Core Debris Retention and Coolability Workshop*, Garching, Germany, March 3-6, 1998, pp. 185-193.
[8] Godin-Jacqmin, L., Bachrata, A., Analysis of the LIVE-L1 experiment with the ASTEC V1.3 code, SARNET/ASTEC report, 2007, CEA/DEN/DTN/STRY/LMA/2007-031.
[9] Buck, M., et al., The LIVE program - results of test L1 and joint analyses on transient molten pool thermal hydraulics, *Progress in Nuclear Energy*, 52, 2010, pp.46-60.
[10] Aksenova, A., et al., Development and application of the CONV code, *Proc. of the RASPLAV Seminar*, Munich, Germany, November 14-15, 2000.
[11] Levin, E. M., et al., Phase Diagrams For Ceramists Vol. 1: Oxides and Salts, American Ceramic Society, 1986, ISBN-10: 0916094049.
[12] Asmolov, V., RASPLAV Project: Major Activities and Results, *Proc. of the RASPLAV Seminar*, Munich, Germany, November 14-15, 2000.
[13] Flemmings, M.C., Solidification processing. Materials Science and Engineering Series, 1974, pp. 59–66.